AUT Journal of Mechanical Engineering

AUT J. Mech. Eng., 10(2) (2026) 167-178
DOI: 10.22060/ajme.2025.24353.6195

Experimental Study on Stall Cell Formation in High-Wing Commercial Jet under Take-Off Conditions

Hamed Rezaei, Mostafa Kazemi, Mahmoud Mani*, MohammadAli Vaziri, Alireza Jahangirian

Department of Aerospace Engineering, Amirkabir University of Technology, Tehran, Iran.

ABSTRACT: This study investigates the flow physics of a high-wing regional jet aircraft under stall conditions. The main aim of this research is to study the effects of nacelle-pylon configuration and trailing edge control surfaces on flow characteristics, particularly the formation of stall cells, during the takeoff and landing phases of the flight envelope. Oil flow visualization techniques were employed to conduct experiments in a low-speed subsonic wind-tunnel at low Reynolds numbers, with angles of attack ranging from 0° to 20°. The study also explored the influence of forced transition achieved by using trip strips, flow physics at different angles of attack, and two slotted trailing edge flaps with deflection angles of 15° and 40° on flow separation. Results from multiple wind-tunnel tests revealed the existence of mushroom-shaped structures, knowns as stall cells, on the wing surfaces of the typical jet aircraft. The size and strength of these structures increased by increment of the angles of attack. Additionally, the slotted flap effectively mitigated stall cell formation by injecting high-pressure flow through the slot and modifying the wing's effective camber line.

Review History:
Received: Jul. 07, 2025
Revised: Aug. 19, 2025
Accepted: Sep. 15, 2025
Available Online: Sep. 17, 2025

Keywords:
Wind-Tunnel Testing
Experimental Analysis
Oil Flow Visualization
Trailing-Edge Flap
Stall Cells

1- Introduction

Flow separation leading to stall imposes considerable performance penalties on lifting surfaces. The resulting loss of lift and malfunctioning of control surfaces can lead to a loss of control, potentially causing critical situations such as spins. These abrupt consequences of stall phenomena can have severe, even fatal, impacts in the aviation industry [1, 2]. Therefore, a deeper understanding of this phenomenon is essential. Decades of research have been devoted to the physics of stall on airfoils [3-5] and wings [6-8]. However, due to factors such as the interaction between wing and body flow, span wise flow caused by wing geometry or wingtip vortices, the influence of leading and trailing-edge devices, and the presence of pylons and engines under the wing, the flow behavior around an aircraft wing is complex and often unpredictable. Consequently, supplementary studies on aircraft models are both valuable and essential. In this context, Gaspari and Moens [9] numerically studied the effect of a morphing droop nose (DN) on the stall behavior of a typical regional jet aircraft equipped with a trailing-edge (TE) flap during takeoff and landing phases. Their findings showed that the DN increased the maximum lift coefficient by up to 10% during takeoff and 15% during landing, delaying stall by approximately 2.5° and 5°, respectively. Additionally, they observed separated mushroom-shaped zones at the flap tip area and vortical cells at the body-wing junction, both of which were significantly controlled with the use of DN. Goc et al. [10] investigated the flow over the JAXA Standard Wing-Body Model (JSM) using numerical methods. They reported that as the AOA increased to the stall point, two separation zones were identified: one at the wingtip and another at the trailing edge of the inner wing near the body. They also reported that the engine nacelle and pylon contributed to vortex formation on the wing. However, due to the implementation of leading-edge (LE) slats and TE flaps, the flow generally remained attached to the wing. In another study on the JSM model, Yokokawa et al. [11] studied the effects of two different nacelle configurations on the flow field around the wing, focusing on stall characteristics through wind tunnel testing. They observed vortical cells on the wing bay and wingtip and found that, at post-stall angles of attack, both nacelle configurations caused large separations on the wing due to interactions between the wing and nacelle-pylon. They concluded that the short-cowling configuration delayed stall and reduced aerodynamic interaction between the wing and nacelle-pylon when compared to the long-cowling model. Additionally, a TE separation at the wing-body junction was observed in the short-cowling configuration at post-stall angles of attack. Zhang et al. [12] used CFD simulations to study the flow separation on the wing of a low-wing commercial jet caused by the nacelle-pylon and explored various strake configurations to control and delay the stall phenomenon. They reported that the nacelle's blockage effect can lead to early separation, which expands across the inner

*Corresponding author's email: mani@aut.ac.ir

wing as the AOA increases. They concluded that an optimally designed strake can generate a stabilizing vortex, which controls separation over the wing and delays stall by up to 3°, while also increasing the maximum lift coefficient by approximately 0.3. Koklu et al. [13] experimentally examined the effects of the nacelle-pylon, LE slat, and TE flap on flow characteristics around the conventional CRM-HL model during landing conditions. They identified multiple unsteady flow structures over the wing, particularly in areas such as the wingtip, the interaction zone between the inner flap and fuselage, and downstream of the pylon installation location using surface flow visualization techniques. These flow structures intensified with increasing AOA. Additionally, they observed localized separated regions near the slat brackets due to wake interactions with the adverse pressure gradient. However, further downstream toward the TE, the high-momentum flow exiting from the flap slot effectively controlled boundary layer growth, ultimately reducing separation in these regions. Despite extensive research on the flow physics around commercial jets, significant uncertainties remain due to the unpredictable and complex nature of flow behavior, particularly in the formation of stall cells. While most research has focused on low-wing aircraft with swept wings, typical configurations in commercial jets, other configurations also merit in-depth investigation. Additionally, many studies have primarily assessed aerodynamic performance, often overlooking a detailed experimental analysis of flow physics. Addressing these gaps could enable more effective designs and improvements. The purpose of this research, therefore, is to investigate the effects of the nacelle-pylon and TE control surfaces on flow characteristics over a high-wing regional jet aircraft during the takeoff and landing phases of the flight envelope. This study utilizes wind-tunnel tests to analyze these effects, with particular attention to unsteady span wise flow and the development of stall cells over the wing, captured using oil flow visualization techniques. Additionally, this research examines the effects of Reynolds number, AOA, trip strip deployment, and flap deflection angle on flow physic.

2- Methodology and Experimental Setup

This study investigates the flow characteristics, particularly the phenomenon of stall cells, using wind-tunnel flow visualization techniques on a scaled aircraft model. Tests are conducted at Reynolds numbers of 82×10^3, 110×10^3 and 137×10^3, calculated based on the free-stream velocity and a mean aerodynamic chord of 0.0468 m. The experiments focus on examining the effects of varying the AOA and applying a trip strip on flow behavior. Additionally, two TE flaps with different deflection angles are manufactured and installed on the model to analyze their impact on flow separation. The parameters studied in this investigation are summarized in Table 1.

The model used in this study is a scaled (1:40) high-wing regional jet with a T-tail empennage, measuring a maximum length of 0.6819 m. The wing, with an aspect ratio of 11.7, includes a non-tapered inner section and a larger outer section with a tapered trailing edge, along with blended winglets at the tips. The wing's overall span and area are approximately 0.6825 m and 0.0398 m², respectively. To ensure precision with smooth curves and edges, the model was manufactured using 3D printing technology with an accuracy of 0.1 mm. Constructed from polylactic acid (PLA), a lightweight thermoplastic known for its high tensile strength compared to other 3D printing materials, the model is well-suited for wind tunnel experiments. To reinforce rigidity and enhance bending resistance, metal structures were incorporated within the wing and fuselage. Additional refinement steps, including sanding, applying polyester putty, and painting, were performed to improve the overall quality of the model. The experiments were conducted at the DANA Aerodynamic Laboratory's low-speed, open-circuit wind-tunnel at Amirkabir University of Technology. The wind tunnel is equipped with a nozzle featuring a 9:1 contraction ratio and a rectangular test section with a cross-sectional area of 1×1 m^2 and a length of 2 m. At a maximum angle of attack of 20°, the model's maximum blockage ratio is approximately 2.5%. Turbulence intensity is maintained at about 0.1% using honeycombs and multiple screen layers. The free stream velocity is measured by an MP120 KIMO portable micromanometer with a precision

Table 1. Different parameters studied in the experiment.

Parameter	Values
Free-stream velocities	30, 40, 50 (m/s)
Reynolds numbers	82×10^3, 110×10^3, 137×10^3
Angles of attack	0, 5, 10, 15, 20°
Flap deflection angles	15, 40°

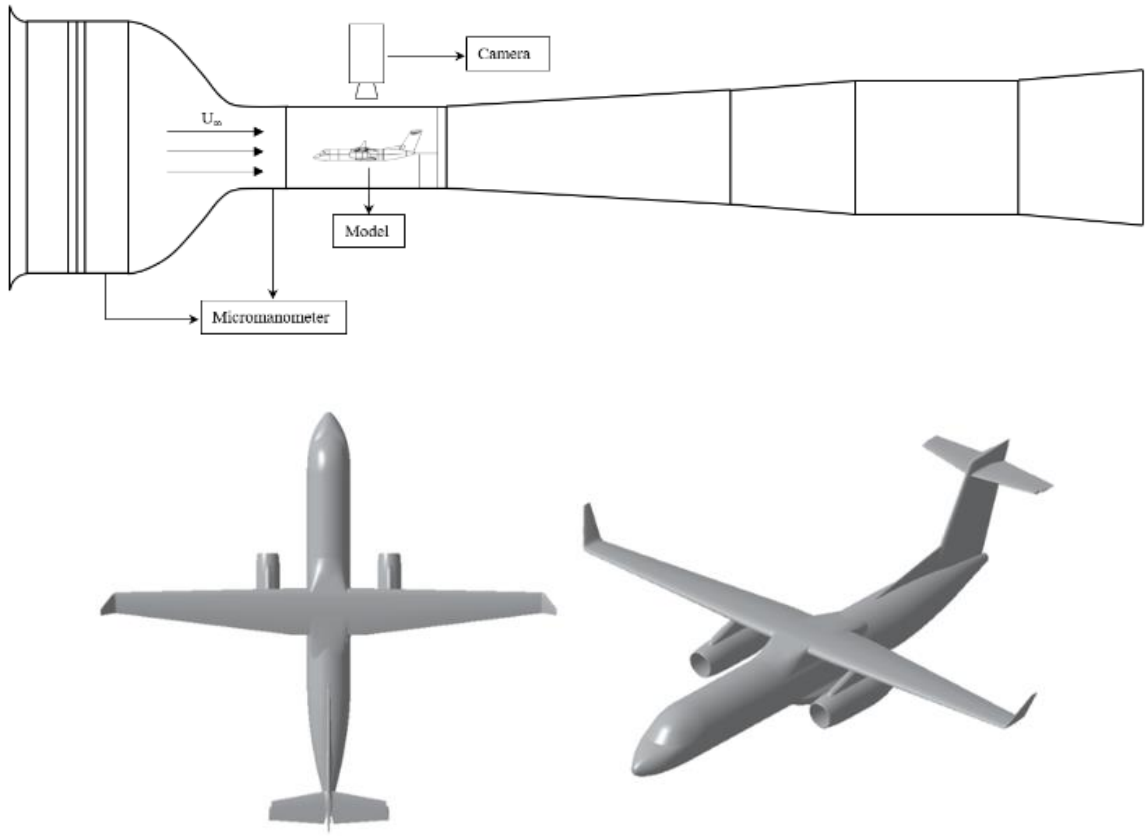

Fig. 1. Schematic representation of the wind tunnel and experimental facilities (up) and CAD model of the aircraft (down).

of 1 Pa. The model's angle of attack was adjusted using a magnetic digital protractor with a precision of 0.1°. To capture detailed surface flow patterns, a Canon 6D camera with a Sigma 24mm f/1.4 DG HSM wide lens was used, set to an ISO of 3200, a shutter speed of 1/30 s, and an aperture of 5.6. Positioned on a digital stand and aligned perpendicularly to the test section, the camera captures top-view photographs of the model. The CAD representation of the examined model, along with schematics of the wind-tunnel and experimental setup, are presented in Figs. 1.

To observe flow characteristics close to the model's surface, an oil film technique was employed, which visually represents streamline patterns adjacent to the wall [14-16]. For these tests, the mixture was prepared by combining specific amounts of TiO_2, paraffin and linseed oils. This method enables continuous observation of separation and reattachment lines, locally stalled regions, and the formation and size of vortical structures along the wing. Additionally, a trip strip which was created from 400-grit sandpaper with an average particle size of 0.2286 mm was applied at X/C = 0.05 following [17] and several preliminary tests. Also, two slotted TE flaps with deflection angles of 15° and 40° were manufactured using 3D printing technology and implemented on the right wing of the aircraft model. Since it is almost impossible to use regular flaps with hinges and actuators for rotation, the flaps were designed and built separately to stand at the designed angle upon installation. Figs. 2 illustrates the schematics of tripped wing and designed TE flaps.

3- Results

To accurately simulate the prototype's boundary layer on the scaled wind tunnel model, the laminar flow must be transitioned to turbulent flow. This ensures realistic flow physics and reliable results. This was accomplished by applying a trip strip at X/C = 0.05 from the wing's leading edge. The trip strip was placed on the right wing, enabling a direct comparison between the tripped and non-tripped wings. Figs. 3 illustrates this setup, with the model positioned at an angle of attack of 0° and Reynolds numbers of 82×10^3, 110×10^3, and 137×10^3. In regions with uniform, high-momentum flow, the oil film is washed away, leaving only traces on the surface. Conversely, areas where oil accumulates indicate zones of low-energy flow or flow separation. This pattern suggests that the flow over the right wing remains attached from the leading edge and only separates near the trailing edge. The trip strip induces turbulence, enhancing the mixing rate of the flow, which draws energy from the free-stream to sustain the boundary layer, thereby delaying separation compared to the left wing. Additionally, at a Reynolds number of 137×10^3, the separation caused by the interaction between the nacelle-pylon and the wing is clearly visible. Observing the left wing, on the right side of the red dashed line, the flow undergoes

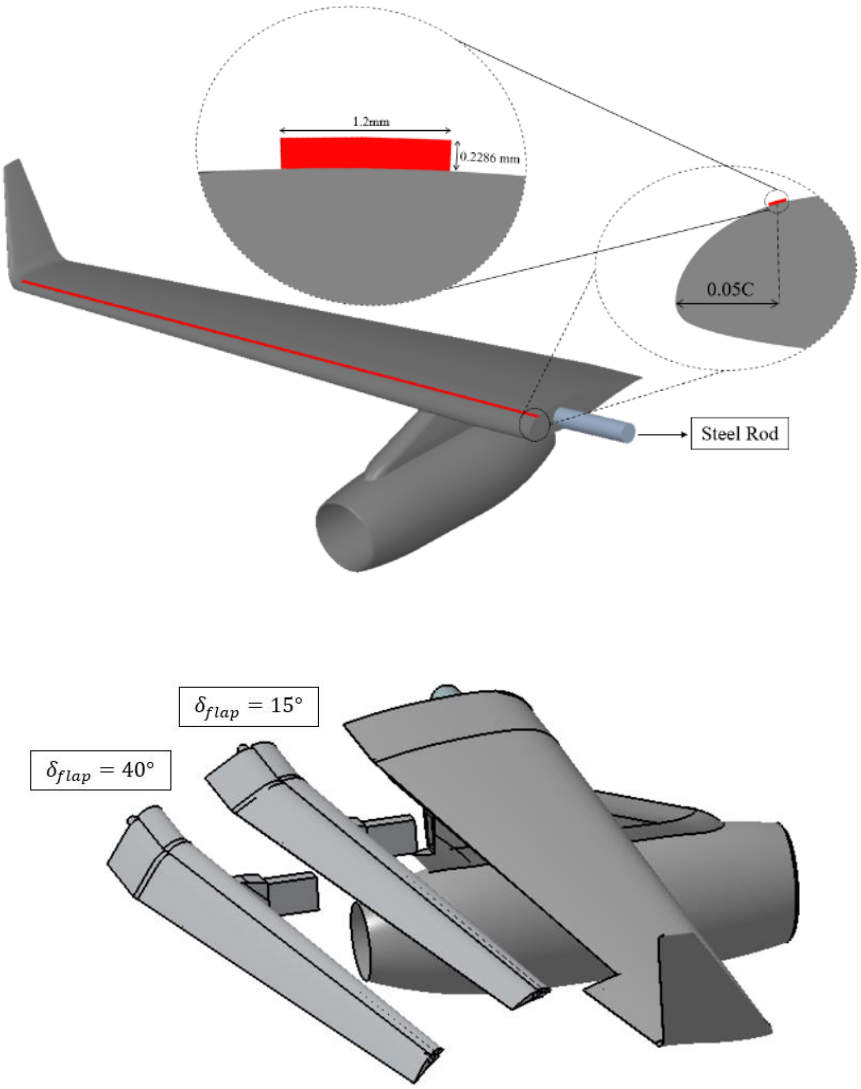

Fig. 2. Schematic representation of the wing equipped with a sandpaper trip strip (up) and TE flaps at δ = 15° and δ = 40° (down).

leading-edge separation before transitioning to turbulent and reattaching to the surface. However, near the trailing edge, the flow separates again as it lacks sufficient momentum to counteract the adverse pressure gradient. In contrast, on the left side of the dashed line, the comparatively lower Reynolds number produces a markedly different flow behavior. At this condition, the reduced momentum of the incoming stream prevents the boundary layer from reattaching to the wing surface once separation occurs, resulting in the development of a fully separated region that extends over a large portion of the chord. Such a flow state is not representative of the actual aerodynamic environment over the prototype wing and therefore introduces significant discrepancies in performance prediction. With increasing Reynolds number, however, the boundary layer gains additional kinetic energy, enabling it to overcome the adverse pressure gradient more effectively. This increase in momentum reduces the extent of the separated zones, allowing the flow to reattach over greater portions of the surface and restoring a more realistic distribution of aerodynamic loads. The observed differences between low- and high-Reynolds-number cases emphasize the critical role of properly modeling the boundary layer transition. In particular, the application of the force transition method ensures that the simulated flow captures the correct onset and progression of transition, thereby improving the fidelity of boundary layer development and producing flow patterns that align more closely with the true aerodynamic behavior of the wing.

To examine the effect of Reynolds number on flow behavior, particularly on stall cell formation, Figs. 4 presents three photographs at an angle of attack of 10° and Reynolds numbers of 82×10^3, 110×10^3, and 137×10^3. At this AOA,

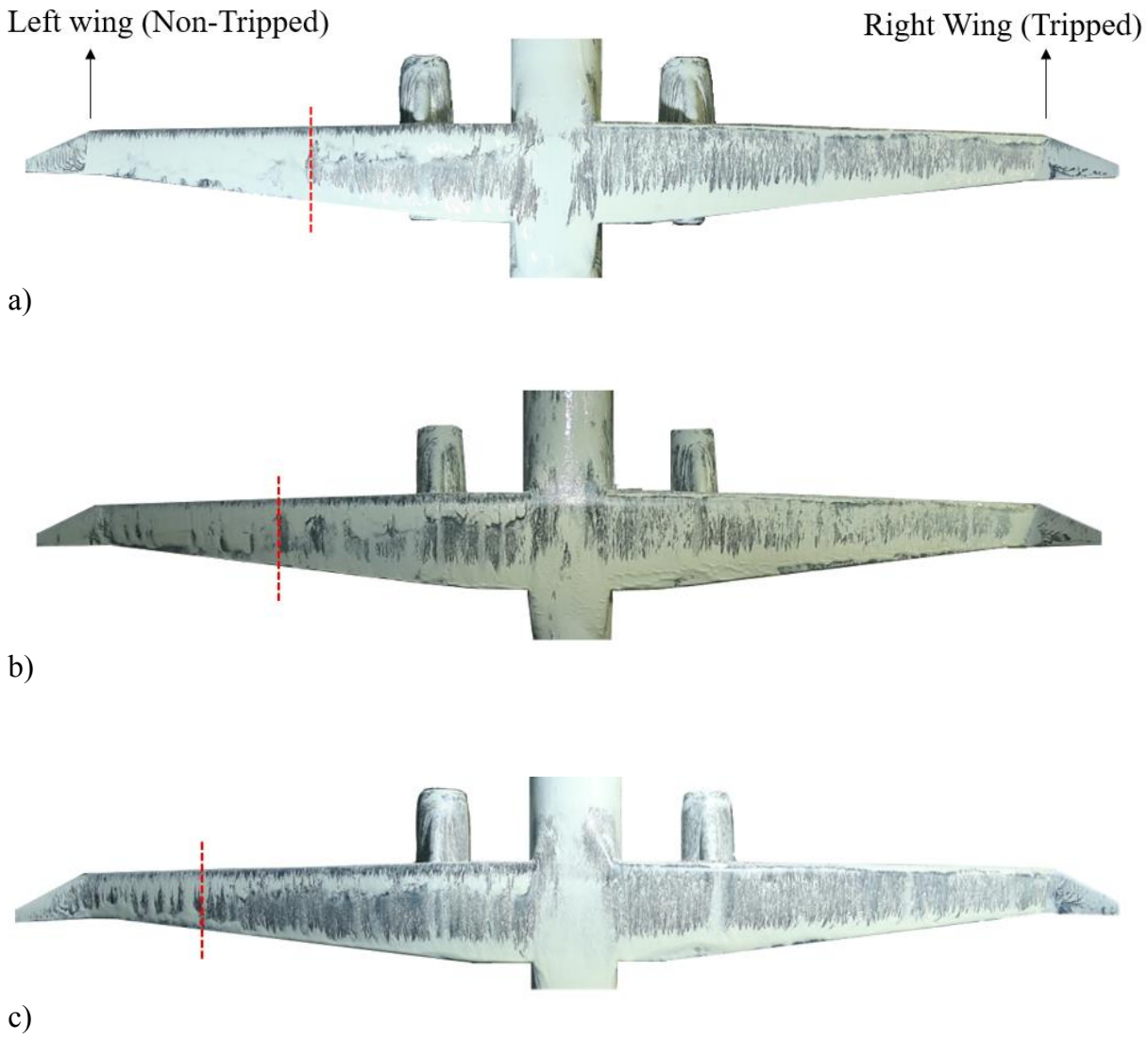

Fig. 3. Top view photographs of the model with trip strip at AOA = 0° and a) Re=82×10³, b) Re=110×10³ and c) Re=137×10³

the wing is near its stall point, leading to multiple separated zones and the development of vortical and span wise flow structures. For Re = 82×10³, a prominent counterclockwise stall cell appears near the trailing edge, between the fuselage and engine pylon, likely due to vortex interactions where the wing meets the body and pylon. Additionally, a spanwise structure is visible along the trailing edge of the outer wing. As the Reynolds number increases to 110×10³, the trip strip is removed to prevent premature leading-edge separation. The increased free-stream momentum helps the flow overcome the adverse pressure gradient, resulting in more robust flow attachment and a significant reduction in separation areas. The previous counterclockwise stall cell eventually loses coherence and breaks down, leading to the development of an extended flow separation zone along the trailing edge of the wing. As this occurs, the well-organized span wise structure that was previously sustained near the outer trailing edge dissipates, and instead, a localized mushroom-shaped stall cell emerges just beyond the nacelle-pylon junction. At a Reynolds number of Re = 137×10³, the flow over the majority of the wing surface remains relatively well-attached, yet distinct separated regions are observed. Two prominent mushroom-shaped stall cells appear symmetrically on either side of the nacelle-pylon, while a smaller, but still well-defined, vortical stall cell develops near the wingtip, where the aerodynamic loading is more sensitive to flow separation. These mushroom-shaped stall cells are characteristic of wings undergoing trailing-edge stall and represent a complex three-dimensional separation phenomenon. Structurally, they consist of two pairs of counter-rotating vortices interconnected by a spanwise flow, which contributes to their stability and persistence. Their footprint can spread across significant

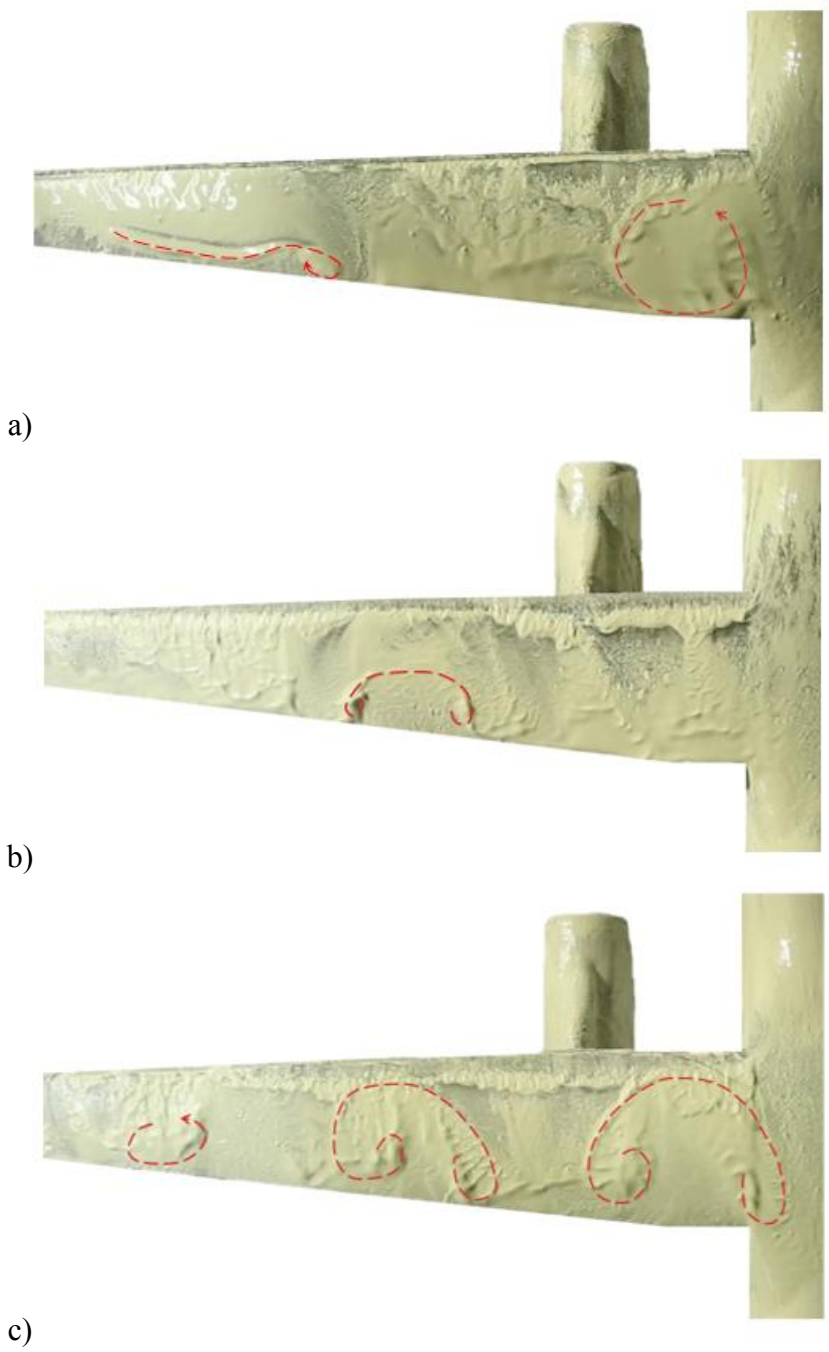

Fig. 4. Top view photographs of the model at AOA = 10° and a) Re=82×10^3, b) Re=110×10^3 and c) Re=137×10^3.

portions of both the wing and adjacent fuselage, introducing unsteady aerodynamic forces. The associated pressure fluctuations and vortex interactions impose intense buffeting loads, which not only degrade aerodynamic performance but may also compromise flight stability and control authority if left unchecked [18, 19].

To deepen the understanding of flow physics in stall and post-stall conditions, particularly regarding the influence of AOA on stall cell formation, Figs. 5 presents the visualization test results at Re = 137×10^3 and angles of attack of 12°, 15°, and 20°. For case (a), the wing experiences stall, with flow separation covering most of the wing's surface except near the trailing edge of the outer section. A small mushroom-shaped stall cell appears at the wing-body junction near the leading edge, likely generated by the interaction between the wing and fuselage flow fields. In addition, a larger stall cell

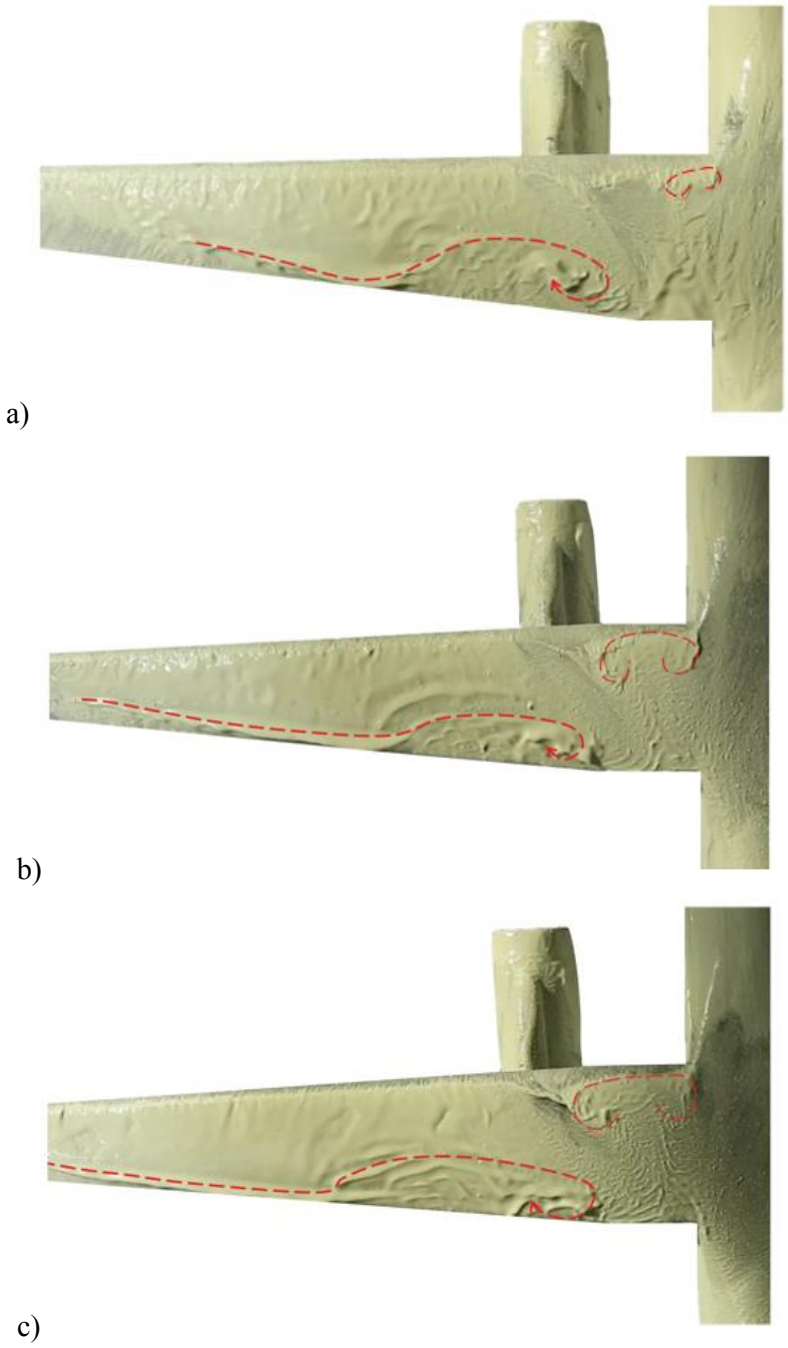

Fig. 5. Top view photographs of the model at Re = 137×10^3 and a) AOA = 12°, b) AOA = 15° and c) AOA = 20°..

extends from the nacelle-pylon area toward the outer wing. This stall cell shows a swirl on one side, caused by separation near the nacelle-pylon, while the opposite side aligns with the reattachment line and exhibits span wise flow toward the trailing edge. As the angle of attack increases, both stall cells grow in size and intensity. For case (c), the mushroom-shaped stall cell expands to cover the entire leading-edge span of the inner wing, with more pronounced swirls indicating stronger rotational flow. The second stall cell also grows significantly, stretching across a larger span toward the wingtip. These developments are likely due to the growth of separated layers from the leading and trailing edges as the angle of attack increases. According to [20], the interaction of these separated shear layers facilitates the formation of mushroom-shaped stall cells.

One of the most common control surfaces used on

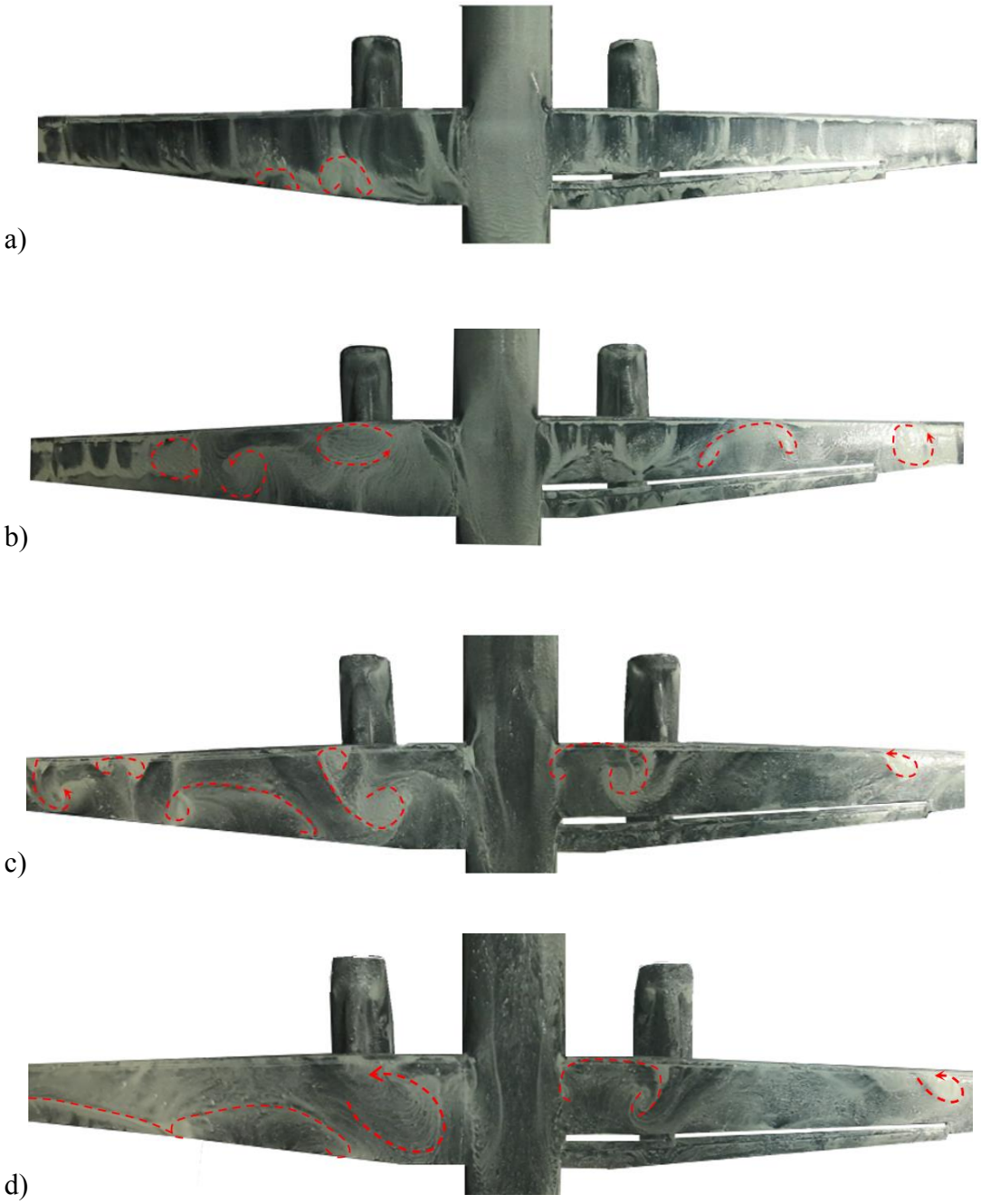

Fig. 6. Top view photographs of the model with δflap = 15° and Re = 137×10³ for: a) AOA = 5°, b) AOA = 10°, c) AOA = 15° and d) AOA = 20°.

commercial jets is the trailing edge flap. To analyze the effects of these flaps on stall cell formation and vortical structures, the right wing of the model is equipped with trailing-edge flaps set at deflection angles of 15° and 40°, allowing for direct comparison with the clean (unflapped) left wing under identical test conditions. The investigation spans a range of angles of attack from 5° to 20°, covering both pre-stall and post-stall conditions. The results, presented in Figs. 6 and 7, demonstrate the impact of flap deflection on flow separation and stall cell behavior for a Reynolds number of 137×10³. As can be seen, both deflected flaps have significantly controlled the stall cells due to changes in pressure distribution over the wing, which bend the streamlines downward and help keep the flow attached. Additionally, a high-pressure flow is injected through the flap slot at the rear end of the wing, increasing resistance to flow separation. For instance, at AOA of 5°, flap deployment results in the disappearance of small stall cells at the nacelle-pylon installation location. At higher angles of attack, where there are several large stall cells over the wing, the flap shows promising results by

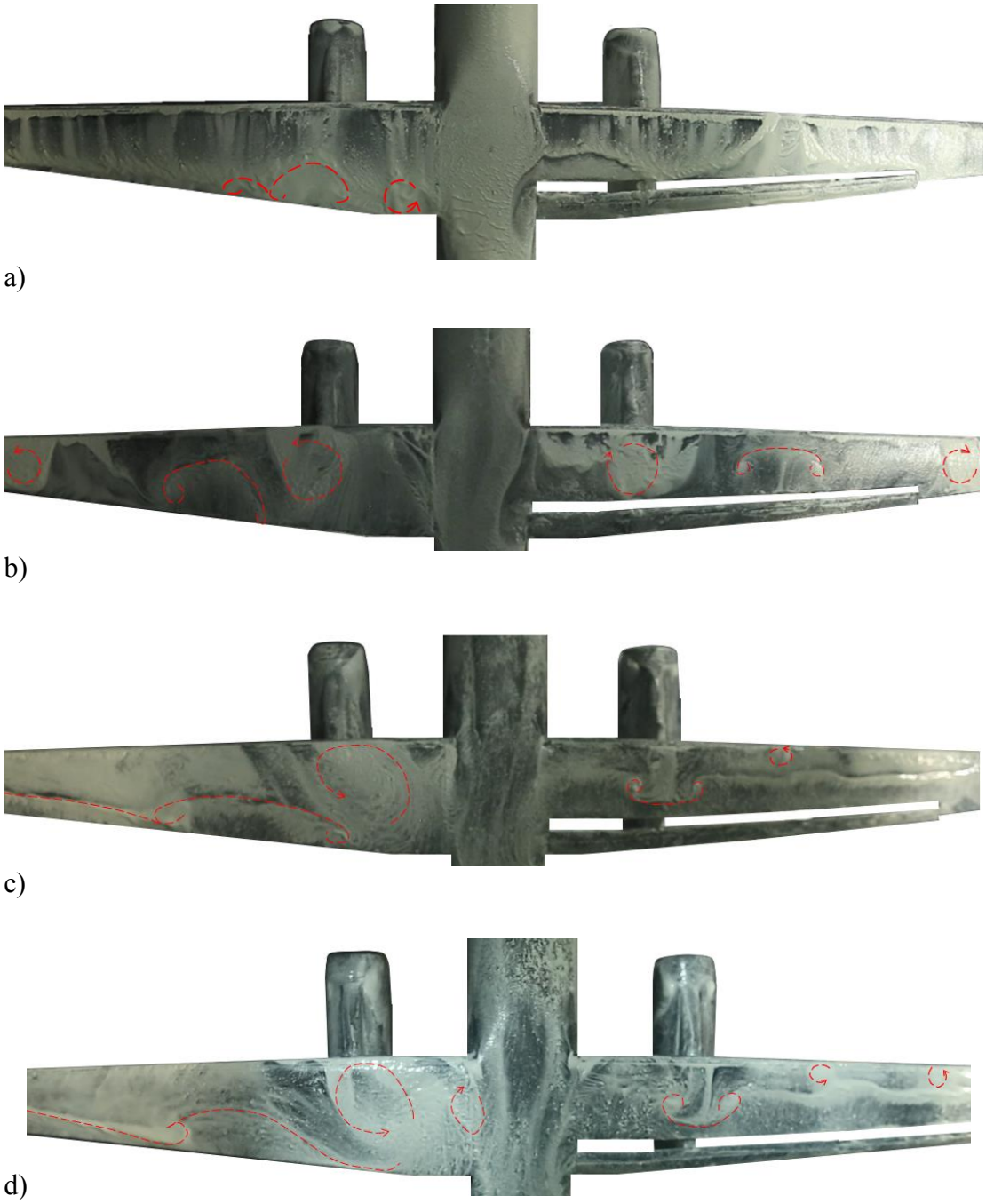

Fig. 7. Top view photographs of the model with δflap = 40° and Re = 137×10³ for: a) AOA = 5°, b) AOA = 10°, c) AOA = 15° and d) AOA = 20°

reducing the number and size of stall cells, especially those located at the trailing edge. It is evident that both deflected flaps improve the flow behavior over the wing, However, the effects of the two flap deflections (15° and 40°) differ significantly. At a 15° deflection angle, the flow remains largely attached across the entire wing surface, showing minimal separation even at high angles of attack. Conversely, a 40° flap deflection, while still beneficial at lower AOAs, leads to notable separated zones and a continuous separation line as the angle of attack increases, particularly at AOAs of 15° and 20°. This occurs because the higher flap deflection increases the wing's effective camber line angle significantly therefore strengthens the adverse pressure gradient along the wing surface. At high AOAs, this adverse pressure gradient overpowers the near-wall flow momentum, preventing the flow from following the wing surface and resulting in flow separation. Thus, while both flap settings improve flow behavior over the wing, the 15° flap deflection proves to be more effective in maintaining attached flow, especially under high-lift, high-angle conditions.

4- Conclusion

In this study, the flow physics over a scaled regional jet aircraft model, particularly the formation of stall cells, were investigated through a series of flow visualization experiments. Conducted in a low-speed subsonic wind-tunnel, these tests explored flow behavior at Reynolds numbers of 82×10^3, 110×10^3, and 137×10^3, and at angles of attack ranging from 0° to 20°, representing conditions relevant to landing and takeoff phases of the flight envelope. The study experimentally examined the effects of forced transition through trip stripping and two slotted TE flaps with deflection angles of 15° and 40° on flow separation. Key findings of the study include the following:

- The trip strip fixes the transition location on the wing, prevents unrealistic early separations, and aligns the boundary layer of the test model with that of the prototype.
- At an AOA of 10°, increasing the Reynolds number prevented flow separation over the entire wing. However, interactions between the wing, fuselage, and nacelle-pylon led to the formation of two mushroom-shaped stall cells on the wing.
- As the AOA increases, both the size and strength of stall cells grow due to the intensified interaction of separated shear flows from the LE and TE.
- The slotted TE flap significantly suppresses stall cells, especially those near the TE, by injecting a high-pressure flow through the slot and altering the effective camber line of the wing.
- Both flaps demonstrated promising results; however, the 40° flap, due to its high deflection angle and limited free stream momentum, caused flow separation on the wing at high angles of attack.

Nomenclature:

AOA	Angle of Attack
CAD	Computer Aided Design
MAC	Mean Aerodynamic Chord (m)
Re	Reynolds number
U_∞	Free-stream velocity (m/s)
δ_{flap}	Flap Deflection Angle

Conflict of Interest

All authors declared no potential conflicts of interest with respect to the research, authorship, and publication of this article.

Acknowledgments

The authors gratefully acknowledge all the members of the DANA research laboratory.

References

[1] C. Belcastro, J. Foster, Aircraft loss-of-control accident analysis, in: AIAA Guidance, Navigation, and Control Conference, 2010, pp. 8004.

[2] M.S. Reveley, J.L. Briggs, J.K. Evans, C.E. Sandifer, S.M. Jones, Causal factors and adverse conditions of aviation accidents and incidents related to integrated resilient aircraft control, 2010.

[3] W. Sears, Some recent developments in airfoil theory, Journal of the Aeronautical Sciences, 23(5) (1956) 490-499.

[4] N. Gregory, C. O'reilly, Low-speed aerodynamic characteristics of NACA 0012 aerofoil section, including the effects of upper-surface roughness simulating hoar frost, (1970).

[5] C. Ostowari, D. Naik, Post-stall wind tunnel data for NACA 44XX series airfoil sections, Texas A and M Univ., College Station (USA). Dept. of Aerospace Engineering, 1985.

[6] E. Kisielowski, M. Mc Veigh, A design summary of stall characteristics of straight wing aircraft, (1971).

[7] S.A. Yon, J. Katz, Study of the unsteady flow features on a stalled wing, AIAA journal, 36(3) (1998) 305-312.

[8] C.W. Harper, R.L. Maki, A review of the stall characteristics of swept wings, (1964).

[9] A. De Gaspari, F. Moens, Aerodynamic Shape Design and Validation of an Advanced High-Lift Device for a Regional Aircraft with Morphing Droop Nose, International Journal of Aerospace Engineering, 2019(1) (2019) 7982168.

[10] K.A. Goc, O. Lehmkuhl, G.I. Park, S.T. Bose, P. Moin, Large eddy simulation of aircraft at affordable cost: a milestone in computational fluid dynamics, Flow, 1 (2021) E14.

[11] Y. Yokokawa, M. Murayama, M. Kanazaki, K. Murota, T. Ito, K. Yamamoto, Investigation and improvement of high-lift aerodynamic performances in lowspeed wind tunnel testing, in: 46th AIAA Aerospace Sciences Meeting and Exhibit, 2008, pp. 350.

[12] W. Zhang, H. Chen, Y. Zhang, S. Fu, Y. Chen, Y. Li, T. Zhou, Numerical Research of the Nacelle Strake on a Civil Jet, ICAS2012, (2012).

[13] M. Koklu, L.G. Pack Melton, J.C. Lin, J. Hannon, M. Andino, K. Paschal, V.N. Vatsa, Surface flow visualization of the high lift common research model, in: AIAA Aviation 2019 Forum, 2019, pp. 3727.

[14] M. Mani, P. Render, Experimental investigation into the aerodynamic characteristics of airfoils with triangular and star shaped through damage, in: 23rd AIAA Applied Aerodynamics Conference, 2005, pp. 4978.

[15] P.M. Render, S. de Silva, A.J. Walton, M. Mahmoud, Experimental investigation into the aerodynamics of battle damaged airfoils, Journal of aircraft, 44(2) (2007) 539-549.

[16] P.M. Render, M. Samaad-Suhaeb, Z. Yang, M. Mani, Aerodynamics of battle-damaged finite-aspect-ratio wings, Journal of Aircraft, 46(3) (2009) 997-1004.

[17] J.B. Barlow, W.H. Rae, A. Pope, Low-speed wind tunnel testing, John wiley & sons, 1999.

[18] K.J. Disotell, Low-frequency flow oscillations on stalled wings exhibiting cellular separation topology, The Ohio State University, 2015.

[19] A. Winkelmann, An experimental study of separated flow on a finite wing, in: 7th Atmospheric Flight Mechanics Conference, 1981, pp. 1882.

[20] D. Weihs, J. Katz, Cellular patterns in poststall flow over unswept wings, AIAA journal, 21(12) (1983) 1757-1759.

HOW TO CITE THIS ARTICLE

H. Rezaei, M. Kazemi, M. Mani, M. A. Vaziri, A. R. Jahangirian, Experimental Study on Stall Cell Formation in High-Wing Commercial Jet under Take-Off Conditions, AUT J. Mech Eng., 10(2) (2026) 167-178.

DOI: 10.22060/ajme.2025.24353.6195